Lab on a Chip

PAPER

View Article Online
View Journal

Cite this: DOI: 10.1039/c7lc00633k

Multimode smartphone biosensing: the transmission, reflection, and intensity spectral (TRI)-analyzer

Kenneth D. Long,[a] Elizabeth V. Woodburn,[a] Huy M. Le,[bc] Utsav K. Shah,[d] Steven S. Lumetta[bc] and Brian T. Cunningham*[ab]

We demonstrate a smartphone-integrated handheld detection instrument capable of utilizing the internal rear-facing camera as a high-resolution spectrometer for measuring the colorimetric absorption spectrum, fluorescence emission spectrum, and resonant reflection spectrum from a microfluidic cartridge inserted into the measurement light path. Under user selection, the instrument gathers light from either the white "flash" LED of the smartphone or an integrated green laser diode to direct illumination into a liquid test sample or onto a photonic crystal biosensor. Light emerging from each type of assay is gathered *via* optical fiber and passed through a diffraction grating placed directly over the smartphone camera to generate spectra from the assay when an image is collected. Each sensing modality is associated with a unique configuration of a microfluidic "stick" containing a linear array of liquid chambers that are swiped through the instrument while the smartphone captures video and the software automatically selects spectra representative of each compartment. The system is demonstrated for representative assays in the field of point-of-care (POC) maternal and infant health: an ELISA assay for the fetal fibronectin protein used as an indicator for pre-term birth and a fluorescent assay for phenylalanine as an indicator for phenylketonuria. In each case, the TRI-analyzer is capable of achieving limits of detection that are comparable to those obtained for the same assay measured with a conventional laboratory microplate reader, demonstrating the flexibility of the system to serve as a platform for rapid, simple translation of existing commercially available biosensing assays to a POC setting.

Received 17th June 2017,
Accepted 24th July 2017

DOI: 10.1039/c7lc00633k

rsc.li/loc

Introduction

Since the introduction of smartphones in 2004, interest in coupling them with wearable devices for monitoring health-related metrics will grow to an over $15 billion per year market[1] focused mainly upon reporting physiological parameters such as heart rate and blood pressure. While the market for such consumer products does not classify the vast majority these sensors as medical devices, there is intense interest in transitioning additional health diagnostics, particularly *in vitro* diagnostic (IVD) tests on bodily fluids from the laboratory to the point-of-care (POC). Tests that can be facilitated through test-specific cartridges that interface with a readout instrument[2,3] or paper-based assays that can be interpreted by visual inspection have obtained regulatory approval that facilitates their use in POC settings.[4,5]

As smartphones continue to include greater computational power and more sophisticated imaging sensors that complement their capabilities for wireless communication and internet connectivity, the interface between IVD testing and mobile devices offers a powerful new POC testing paradigm. The output of nearly all of the most common laboratory-based diagnostic tests can be sensed using a smartphone with sensitivity that rivals that of conventional laboratory-based benchtop instruments. Examples include smartphone-based microscopy,[6,7] fluorimetry,[8,9] Enzyme linked immunosorbent assay (ELISA),[10] polymerase chain reaction (PCR),[11] and lateral flow assays.[12,13] The reader is directed to recent reviews on the topic of smartphone-based biosensing.[14,15] It is evident that while laboratory-based assays and detection instruments provide high throughput and automation, enormous needs exist to provide diagnostic information to people who lack convenient access to a diagnostic test facility. Additionally, in many urgent health situations, an immediate result is required for feedback to the physician and patient.

[a] *Department of Bioengineering, Micro and Nano Technology Laboratory, University of Illinois at Urbana-Champaign, 208 N. Wright Street, Urbana, IL 61801, USA. E-mail: bcunning@illinois.edu*
[b] *Department of Electrical and Computer Engineering, University of Illinois at Urbana-Champaign, USA*
[c] *Coordinated Science Laboratory, University of Illinois at Urbana-Champaign, USA*
[d] *Department of Computer Science, University of Illinois at Urbana-Champaign, USA*

To date, reported examples of smartphone-based IVD detection instruments are only capable of carrying out a single type of analysis, and with a few exceptions[9,16] are capable of very limited multiplexing of tests. The capability for a laboratory-based microplate reader to function as a "multi-mode" instrument has been long recognized as a desirable characteristic that enables a single system to transition between spectrometric absorption analysis (as used in ELISA assays), fluorometric analysis (as used in molecular beacon assays, fluorescent polarization (FP) assays, and luminescence-based assays), and, in the case of one product (PerkinElmer EnSight) label-free optical biosensor assays. The ability of a detection system to easily transition between these modalities enables the user to purchase only one instrument, and to use a common liquid handling format and software interface across a variety of applications.

In this work, we report, to our knowledge, the first example of a smartphone-connected detection instrument that can measure the output of three distinct spectral biosensing modalities using two separate yet complimentary light paths. The three modalities represent a large fraction of all commercially available IVD tests for which a liquid sample changes color, or in which a liquid sample generates light as a visible indicator of the test's outcome. The system is capable of performing spectral analysis of:

Optical transmission

Optical transmission of light through a test sample at specific wavelength(s). This measurement modality is commonly used in ELISA assays, liquid phase plasmonic nanoparticle-based tests including surface plasmon resonance (SPR) and localized surface plasmon resonance (LSPR),[17–19] latex (or other nanoparticle-based) agglutination tests (LAT),[20] and transmissive surface-based SPR, LSPR, and photonic crystal (PC) based tests.[19,21,22] ELISA tests are a mainstay of contemporary biosensing tests, with ready-to-go kits available for thousands of different biological targets.

Reflectance spectroscopy

Reflectance spectroscopy of light against a resonant optical transducer, as used in reflective label-free optical biosensing techniques such as SPR, PC, or reflectometric interference spectroscopy (RIFS). While these direct binding label-free approaches do not currently have commercially available assay kits associated with them, they have been applied to thousands of biological analytes due to their simplicity and speed.[23]

Intensity spectroscopy

Intensity spectroscopy from photon-generating assays such as those based upon fluorescence, chemiluminescence, bioluminescence or quantum-dot (QD) emission. A broad variety of biosensing assays have such a readout, including fluorescence or chemiluminescent immunoassays (FIA, CLIA), fluorescent polarization (FP), Forster resonance energy transfer (FRET) as well as several molecular diagnostics, including polymerase chain reaction (PCR) and related loop-mediated isothermal amplification (LAMP).

Together, we estimate that these modalities can perform the necessary spectral readouts of 90–95% of commercial immunoassays,[24,25] the exception being radioimmunoassays (RIAs). In particular, as traditional ELISAs are being replaced by FIAs and CLIAs,[26] the ability to easily switch between measurement modalities makes this system capable of maintaining utility for a variety of applications, and a useful opportunity to potentially compare different tests for the same analyte on the same point-of-care device.

The spectral transmission-reflectance-intensity (TRI)-analyzer takes advantage of the fact that all three modalities share the requirement to measure changes in the spectrum of light that is either absorbed, reflected, or emitted during the course of each type of IVD test. Our approach allows the user to select from one of two light paths: illumination of the assay with either the internal white LED of the smartphone that is typically used for "flash" exposure photography, or instead with an inexpensive green laser diode. Accurate spectral analysis is performed by collecting light from the assay into an optical fiber, whose distal end directs light through a diffraction grating into the smartphone's rear-facing internal camera. The optical components are arranged wholly within a 3D-printed plastic cradle, containing a slot through which an assay cartridge is inserted.

For many clinically relevant assays, multiple samples, replicates, positive/negative controls, and/or standard calibration solutions are required. Few smartphone-based sensing platforms have demonstrated this capability beyond taking pictures of multiple colored samples and performing RGB-based color processing. By converting the smartphone camera into a spectrometer, we lose the spatial discrimination that would allow simultaneous measurement of multiple samples. Instead, multiplexing is achieved using a cartridge comprised of a linear series of liquid compartments that slides through an opening in the back of the cradle. By pairing this linear motion with the smartphone's ability to capture video, the spatial dimension separating the liquid chambers in the cartridge can be reconstituted with video post-processing, allowing for the rapid and user-friendly measurement of multiple samples with a single motion, similar to swiping the magnetic strip of a credit card across a magnetic read head.

Each sensing modality utilizes a unique cartridge configuration with the same overall form factor. Both transmission and reflection modalities rely on a bifurcated illumination-collection fiber optic assembly that allows light from the smartphone flash to pass through a transparent cartridge and reflect off a stationary mirror positioned within the cradle or interact with a PC biosensor that operates as a wavelength-selective resonant mirror at the cartridge's back wall, which is coated in an opaque dye to prevent reflection by the stationary mirror. The intensity modality uses cartridges with a transparent bottom to allow for orthogonal fluorescent excitation of the sample chambers. All three modalities then collect the reflected light *via* the collecting fiber of the bifurcated fiber assembly which is then transmitted to the rear-facing camera of the smartphone.

Importantly, the detection approach enables the user to "swipe" the cartridge through the instrument while the smartphone records video at 60 frames per second, and software can identify the frames from the video that represent images gathered while the center of each chamber is aligned with the illumination/read head. Thus, the user is freed from the necessity of performing accurate alignment of the cartridge's liquid chambers within the instrument, and the cartridge can be read in a similar manner to the approach used for scanning a credit card past a magnetic stripe reader. Multiplexing in this fashion enables a single cartridge to contain experimental controls, replicates, and a series of active tests.

In this paper, we demonstrate the spectral TRI-analyzer first for representative tests that verify its capabilities to measure liquid absorption spectra, PC biosensor resonant reflection spectra and fluorescence spectra. Then, using commercially available diagnostic assay kits for colorimetric output (ELISA) and fluorescence output, we validate the instrument's two light paths and demonstrate that the spectral TRI-analyzer provides equivalent limits of detection (LOD) for reading the same assay with a commercially available 96-well microplate reader. While there exist many opportunities to optimize assays for use with the TRI-analyzer system, the focus of this work is on the demonstration of ease-of-translation readily adaptable the thousands of existing commercial assays on the market. Diagnostic assay kits for the PC biosensor modality are not commercially available.

We chose our assay application demonstrations to represent tests that have important implications for maternal and neonatal health in developing parts of the world where a POC test would have enormous value. First, we perform an ELISA assay for detection of fetal fibronectin, a biomarker protein test for expectant mothers that is diagnostic for spontaneous pre-term birth. Next, we perform a fluorescence-based assay for phenylalanine, a biomarker used to diagnose phenylketonuria, a life-threatening but manageable genetic condition, in newborns.

Optical design and fabrication

An important design requirement for the TRI-analyzer was to make the approach easily adaptable to any smartphone with a

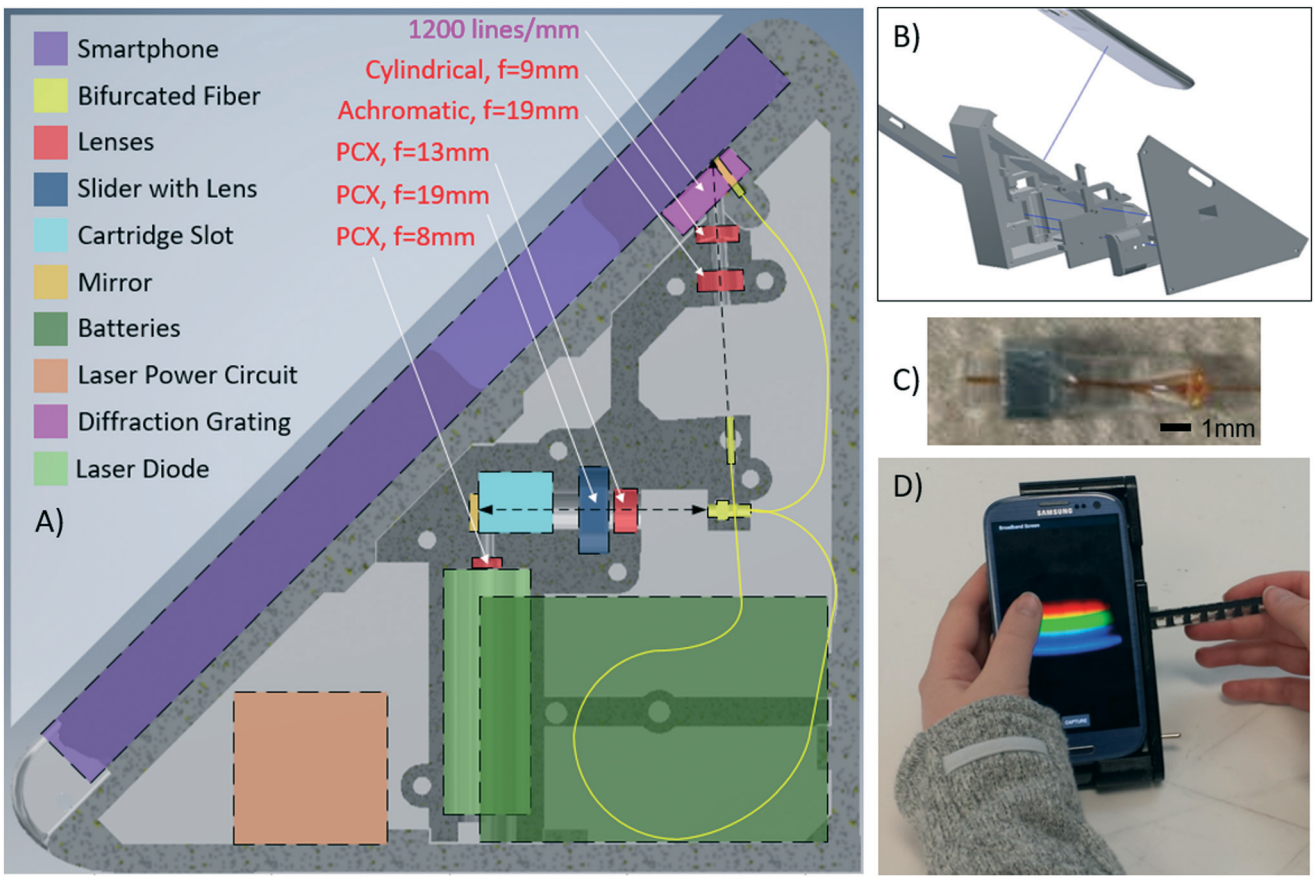

Fig. 1 Design of spectral TRI-analyzer. A) Schematic of internal layout for optical and electrical components. A custom bifurcated fiber (100 μm core with d = 1.8 mm glass capillary tube (proximal) and 2× d = 1.25 mm ceramic ferrules, coastal connections) was used to compact the light path into a handheld device. Fiber is arranged to maximize bend radius, increasing long-term stability. B) 3D CAD model was created, comprised of 5 plastic parts printed *via* stereolithography. Two halves of optical housing maintain lens alignment and optical chamber isolation. All portions of cradle were designed to slide together and attach with M3×0.5 machine screws. C) Glass capillary tube with bifurcated fibers and metal nut used to align the fiber in the cradle. D) Image of final device in use with absorption cartridge.

rear-facing camera and rear-facing flash LED through small mechanical adjustment to the cradle body, but without adjustment of the core optical components. Thus, we chose to use optical fibers to bring light from the LED to the test sample, and to bring light from the test sample to the camera. In principle, the core optical components of the system would be identical for any smartphone, with two simple changes: 1) the phone interface is modified to use the physical dimensions of the phone to align the sensing fiber with the rear-facing camera and 2) the illumination fiber would be routed to collect light from the smartphone flash. As shown in Fig. 1, the distal end of the "illumination" fiber (100 μm diameter, multimode) is placed directly in front of the flash LED to direct white light through the test sample for the transmission and reflectance modalities. The other "sensing" fiber (100 μm diameter, multimode) collects light transmitted through the test sample, reflected from the PC, or emitted by fluorophores at its proximal end and directs it toward the rear-facing smartphone camera, oriented at a 41.3-degree angle. The light emerging from the sensing fiber is collimated by an aspheric lens (EFL = 19 mm) and then focused in the non-spectral dimension with a cylindrical lens (EFL = 9 mm) before passing through a 1200 lines per mm transmission diffraction grating (Edmund Optics 49-578) held within the cradle body directly over the opening of the rear-facing camera. The light is focused to optimize use of the CMOS pixels in the non-spectral dimension allowing for increased sensitivity. The proximal ends of the sensing and illumination fibers are gathered together in a bifurcated configuration, so they are directly adjacent and held within a glass capillary tube that is mounted in a slot within the cradle body. The optical fiber assembly is the only custom-made component of the system, due to the specific fiber length requirements (71 mm for the illumination fiber and 137 mm for the sensing fiber) and ferrules on the distal ends. Due to the accuracy of the

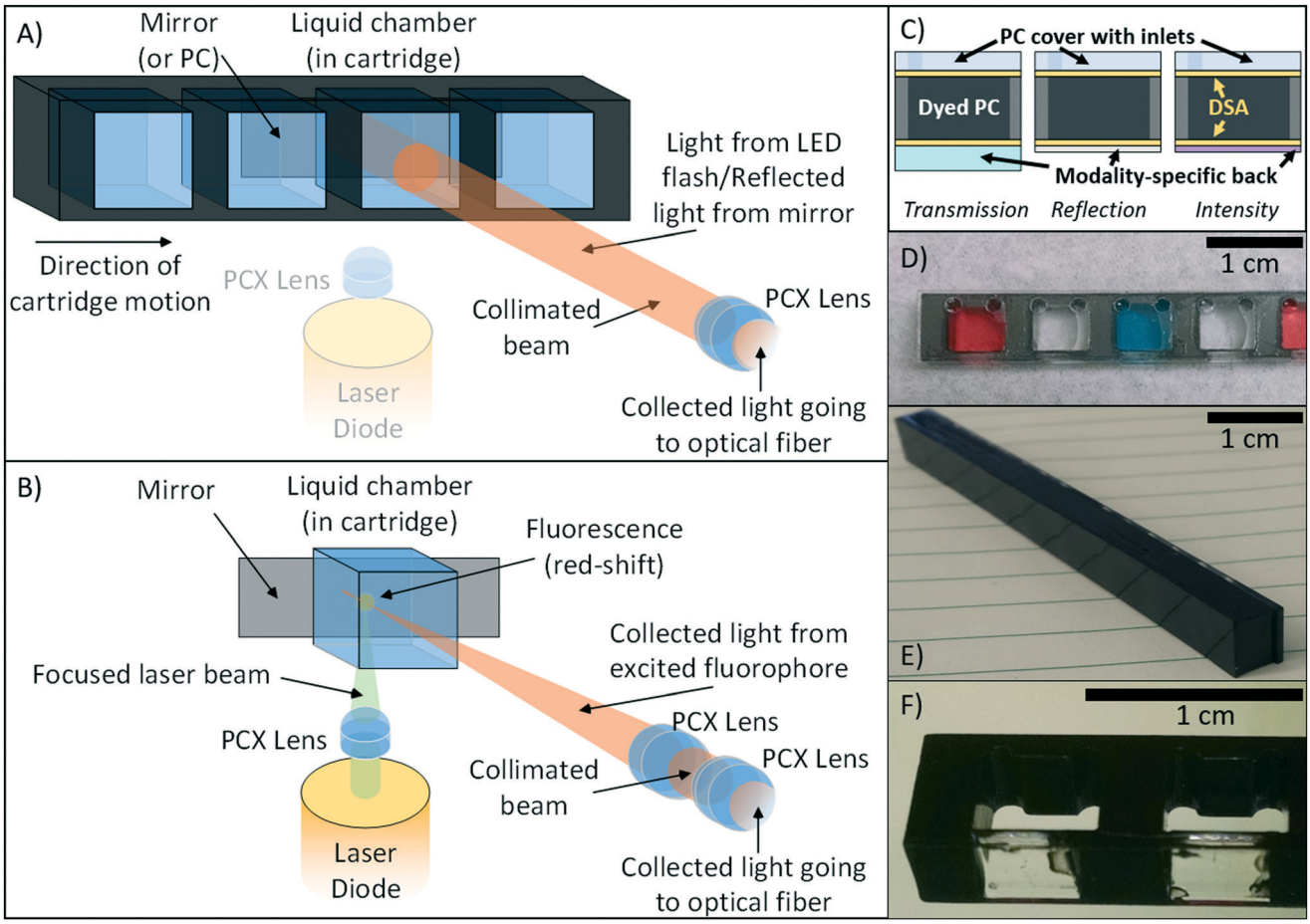

Fig. 2 Two principal light paths and cartridges for each of the three modalities. A) Reflection (PC-only) and transmission (absorption or PC) optical pathway. Collimated light from the on-board smartphone flash is directed through the sample chamber. For reflection-based PC measurements, a back-coated cartridge prevents transmitted light from being collected. For transmission measurements, light is reflected by cradle mirror directed toward the collection fiber. B) Fluorescence/luminescence intensity optical pathway. A laser pointer diode is co-focused to a point near the back-side of the cartridge where the collection fiber is similarly focused *via* addition of a single plano-convex lens into the optical path *via* a SLA-printed slider actuated from outside the cradle. Additional cartridge wells/housing was removed for clarity in B). C) "Sandwich" style cartridge fabrication alternating plastic or glass substrates with double-sided-adhesive (DSA) showing how different backings facilitate different modalities. D) Transmission cartridge showing inlet/outlets and optically-isolated chambers. E) Dyed PC for label-free reflection measurements. F) Close-up of intensity cartridge demonstrating selectively-dyed cartridge body allowing for bottom-illumination with 532 nm laser diode.

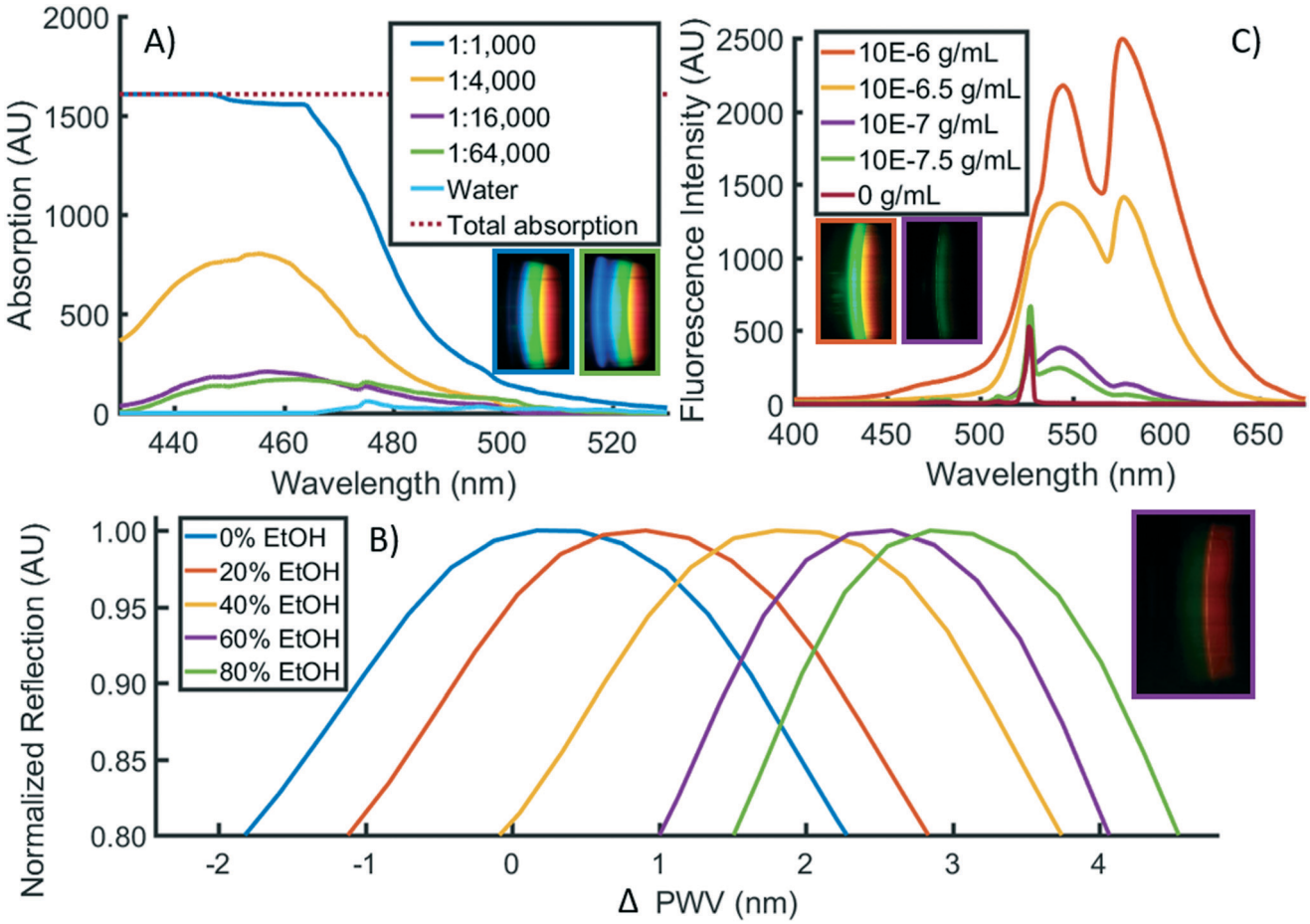

Fig. 3 Qualitative proof-of-concept of 3 principal modalities. A) Transmission. Yellow food dye was diluted in water at concentrations ranging from 1 : 1000 to 1 : 64 000, a 64× concentration range. Absorption was measured by subtracting sample transmission from that of water. Observable absorption occurred in the blue region (400–500 nm) of the spectrum. Inset raw images correspond to concentration of yellow dye of their outline. B) Reflection. 0–80% mixtures of ethanol in water were prepared and introduced into a PC-based cartridge, producing narrowband reflection in the 580 nm range. Measurements of each cartridge chamber filled with water were subtracted from measurements of those chambers filled with ethanol solutions to produce ΔPWV shifts. Inset raw image corresponds to concentration of ethanol of its outline. A central line of pixels was used to produce spectra shown. C) Intensity. R6G dye was diluted in water and excited with the on-board laser diode. Inset raw images correspond to concentration of R6G of their outline.

3D printing technology used to generate the cradle (FormLabs, Form 2 at 50 μm resolution), all optical components (lenses, reflection mirror, optical fiber assembly, and green LED) may be placed into their respective holding locations in correct optical alignment without further modification and minimal tuning of the system with set screws for each of the fiber terminations.

For transmission and reflection modalities the smartphone flash serves as the light source. It is collected by one of the two distal ends of the bifurcated optical fiber, and expanded to a collimated beam with a plano-convex lens (Fig. 2). After passing through the sample chamber, either complete reflection (transmission) or wavelength-selective reflection (reflection) results in the signal passing through the sample once again and being focused on the image of the proximal end of the sensing fiber for transmission or reflection modalities, respectively. The mirror is mounted and aligned inside the cradle, where it serves as the default reflection surface.

For the intensity modality, a 532 nm laser diode (10 mW, 3 V), similar to those found in green laser pointers, is shone orthogonally to the main optical path of the instrument. With the flash turned off, the collecting light path of the instrument is augmented with an additional lens which serves to focus the collection to a point close to the rear face of the cartridge. This lens is inserted into the optical path by pressing a button on the exterior of the cradle, which slides the lens into the correct position. The laser is focused within the test sample at the same point within the cartridge at which the collection lens is also focused to provide for maximal fluorescence collection.

All optical components were optimized *via* non-sequential optical simulation (Zemax), with total optical efficiency prioritized for the intensity modality's optical configuration. The 3D-printed cradle is comprised of two housing pieces held together with steel fasteners to robustly maintain optical alignment. Holes were threaded with an M3 tap, and final clearances of moving parts were adjusted by hand to allow for

smooth sliding before mounting and alignment with machine screws. Optical alignment was completed first with the transmission/reflection light path, and then with the intensity light path, using a cartridge with rhodamine 590 chloride (exciton) laser dye to visualize the optical paths.

The laser diode is powered by a custom circuit providing a constant-current to the diode from three on-board AAA batteries, based on a LED flashlight control circuit (Texas Instruments). This circuit is soldered on a small protoboard, and attached to a switch accessible from the outside of the cradle (visible in Fig. 1D).

To interface with the cradle, custom cartridges were designed to facilitate introduction of samples to the light path. While all based on the same fundamental construction, each modality requires slight modifications to the cartridge design (-Fig. 2C–F). The cartridge bodies for each modality are comprised of a laser-cut acrylic sheet. This acrylic sheet provides the separation between chambers, and the overall structure for the cartridge, which can be modified to support different sample measurement cross-sectional areas, sample volumes, and chamber spacings. For our experiments, we selected a chamber spacing that would allow for user-friendly sample manipulation with an 8-channel multipipette. Laser-cut 50 μm thick double-sided adhesive (DSA) (3M, Optically Clear Adhesive 8212) is applied to both sides and a thin acrylic cover with laser-cut access ports is adhered to the front of the cartridge, as shown in the cross section of Fig. 2C. The back of the cartridge is comprised of glass (transmission cartridges), acrylic film (intensity cartridges), or PC-coated polycarbonate film (reflection cartridges). Depending on the modality, different portions of cartridges are dyed with opaque black dye (Dykem 81724) (Fig. 2E and F) to prevent optical communication between adjacent fluid compartments and to provide a clear boundary between cartridges for automated sensing of the compartments as they pass the illumination/read head during video-based cartridge scanning. To provide consistent positioning of the cartridge in the light path, a copper spring is attached to the collection-end of the cartridge chamber, so the cartridges are pressed firmly against one wall of the cradle's slot.

A custom Android app was developed to assist with data collection. This app sets parameters, including exposure time and focal length, to constant values to provide for inter-assay consistency and to facilitate data collection. After the assay of choice has been completed and is ready to be measured, the App allows the user to choose the number of samples, standards, and replicates before walking the user through collection steps for each liquid chamber and/or cartridge.

Qualitative proofs-of-concept for each of the three modalities were completed with prepared test liquids in the cartridge chambers (Fig. 3). To demonstrate Transmission measurements, we prepared a series of diluted yellow food dye (McCormick) to a range such that measurable optical absorption was observable on the system (~1 : 1000), and then performed serial dilutions to observe concentration-dependent absorbance (Fig. 3A). Note that, as the dye absorbed primarily wavelengths in the blue portion of the spectrum, the blue wavelengths are removed from the image as the dye concentration increases. Difficulties in aligning the sample chamber with the optical path for low concentrations of yellow dye resulted in a high standard deviation, which was addressed with dyed cartridges as shown in Fig. 2D (data not shown). To demonstrate the reflection modality, we used a PC-integrated cartridge and introduced mixtures of 0%, 20%, 40%, 60%, and 80% ethanol (EtOH) in water to manipulate the bulk refractive index of the liquid in contact with the PC (Fig. 3B). Note that only a narrow band of wavelengths are efficiently reflected by the PC into the sensing fiber, representing a narrow bright red band in the spectrum image gathered by the phone's image sensor. A single cartridge was filled with water, followed by the 5 ethanol concentrations to normalize for intra-sensor variation in starting resonance wavelength. By taking the middle row of pixels from the raw images, we observed a clear relationship (R^2 = 0.986) between the change in peak wavelength value (PWV) reflected from the PC with the addition of EtOH solutions and the refractive index of the liquid inside the fluid compartment, corresponding to a 114.0 nm per RIU bulk refractive index sensitivity. Finally, to demonstrate the Intensity modality, we used the laser to excite the fluorescent emission of rhodamine 590 chloride (R6G) (exciton) within a cartridge configured for intensity measurements. The dye was diluted to concentrations between 10^{-6} and $10^{-7.5}$ g mL^{-1}, and

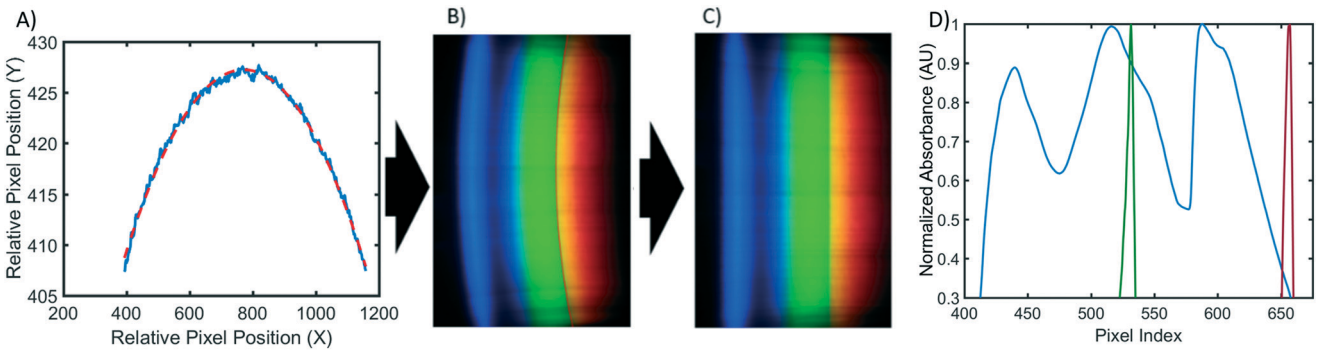

Fig. 4 Spectrum processing. A) Boundary of the red channel is found in every row of the image and a circle is fit (B). C) Straightened spectral image used to generate a single data spectrum. D) Laser pointers are used to determine pixel-to-wavelength conversion as reported previously.

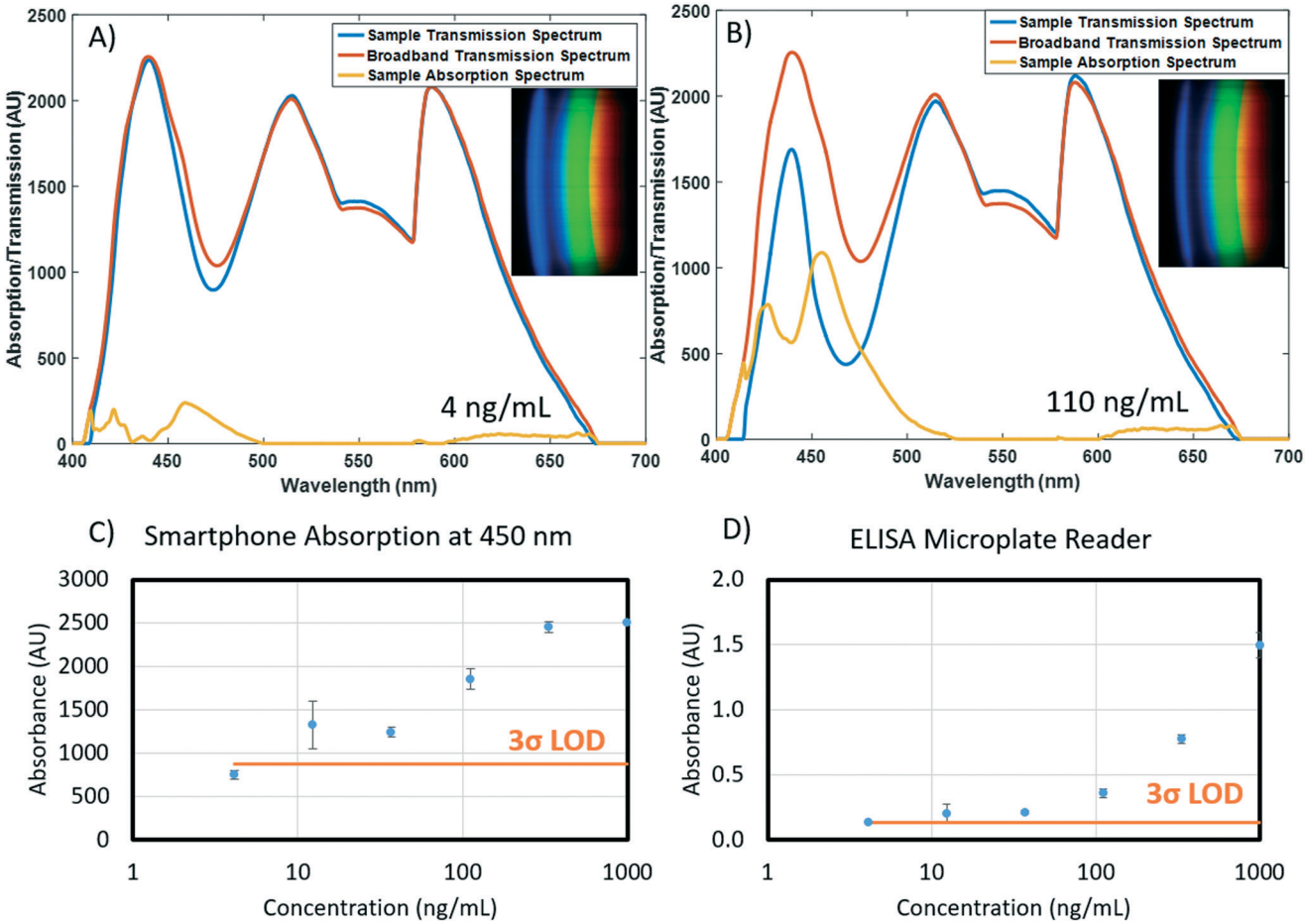

Fig. 5 A) and B) Sample transmission spectra, absorption spectra, and raw RGB image data (insets) for 4 and 110 ng mL^{-1} samples of fFN, respectively. C) and D) Comparative dose–response curves for spectral TRI-analyzer and 96-well microplate reader. Standard concentrations from 4 to 1000 ng mL^{-1} were assayed along with a human serum sample spiked at 50 ng mL^{-1} (not shown). Limit of detection was determined as 3 standard deviations over the mean of zero concentration standard (n = 3).

resultant images were processed to generate fluorescence intensity spectra (Fig. 3C). Note that the green emission from R6G is clearly visible over the entire range of concentrations, the intensity is concentration dependent, and that, due to the orthogonal illumination, a minimal amount of light from the laser diode illumination source is present within the fluorescence emission spectra, even at low R6G concentrations.

Validation of the spectral TRI-analyzer with commercially available diagnostic tests

To demonstrate the capabilities of the system, we selected a representative assay for each light path with a common theme of IVD tests performed in the context of maternal and child health. Recognized as two of the eight Millennium Development Goals (MDGs) by the UN, maternal and child health has remained one of the primary foci of global health strategies. As we transition from the MDGs to the recently released Sustainable Development Goals (SDGs), the WHO released a retrospective analysis of our successes and remaining challenges in the realm of health around the world. From that report, most of the major successes coming out of the health related MDG efforts have been related to infectious diseases, while most of the largest shortfalls are within the realm of maternal and child health. Many countries have initiated subsidized maternal and child health programs, and health outcomes have improved; however, there is significant work to be done to improve outcomes for mothers and children alike, which motivates the specific applications we have selected for this work.[27,28]

Transmission/reflection light path: fetal fibronectin ELISA assay

According to the WHO, over 10% of babies born each year are preterm, and complications arising from these births constitute the single leading cause of death in children under the age of 5.[29] While multiple strategies exist to reduce

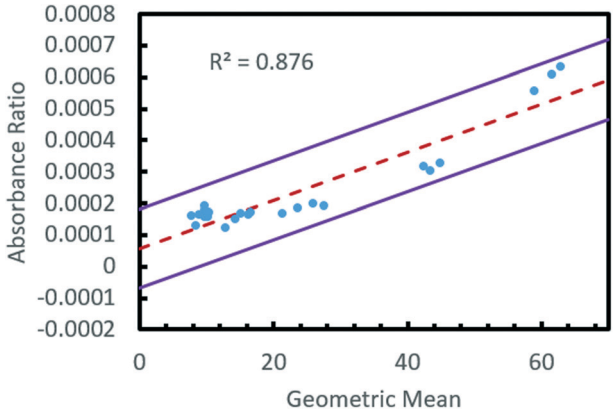

Fig. 6 Bland–Altman analysis of spectral TRI-analyzer compared with standard microplate reader for readout of fFN assay. A variation on the standard Bland–Altman method using the geometric mean and log difference was applied to all non-zero values for each assay (Bland). The log differences showed a dependence on the magnitude of the measurement, so a regressive approach was used to model the relation, as described by Bland (mean of regression shown with dashed line). ±1.96 S.D. limits of agreement are shown as solid lines.

complications associated with preterm births, diagnosis can often be challenging.[30] Fetal fibronectin is a glycoprotein that has a high negative predictive value for spontaneous preterm birth.[31,32] Particularly when combined with a physical measurement of the cervical length, fetal fibronectin is an important diagnostic indicator to facilitate treatment, continued monitoring, or hospital referral of at-risk mothers. While rapid lateral flow-based assays exist, they are not quantitative, and require specialized proprietary readers.[33,34] Serological detection of fFN is routine in a laboratory setting, and the translation of a fFN test to a point-of-care diagnostic would provide useful information to health care providers, particularly with populations at-risk for pre-term births.

For fFN detection, a commercially available ELISA kit was purchased (CUSABIO) and used to generate standard curves, as well as measure spiked serum concentrations within physiologically relevant ranges. Kit reagents were prepared following manufacturer instructions, and reactions were completed in the included 96-well microplate. Standard concentrations were serially diluted and run in triplicate at concentrations ranging from 4 to 1000 ng mL^{-1}. Spiked plasma samples were created at a concentration of 50 ng mL^{-1} from human plasma (n = 3). All samples were added to the microplate, and ELISA steps were completed per manufacturer directions. After the addition of stop solution, the samples were immediately read in a benchtop 96-well plate reader (BioTek, Synergy HT), and then transferred to a sample cartridge with a multichannel pipette.

Filled cartridges were measured using the developed App to take five images of each sample as it was slid through the cartridge slot. The cylindrical lens that extends the non-spectral dimension of spectra onto the image sensor introduces spherical aberration, resulting in a curved appearance of the resultant spectrum images, as shown in Fig. 4A and B. As this is a function of internal optics and not the alignment of the smartphone and the cradle, the curvature observed is constant throughout multiple measurements and multiple phone removals/insertions (data not shown). By fitting the pixel locations of where the red filter drops off (~580 nm) in each spectral row to a circular arc, spectra can be linearized and then summed in the non-

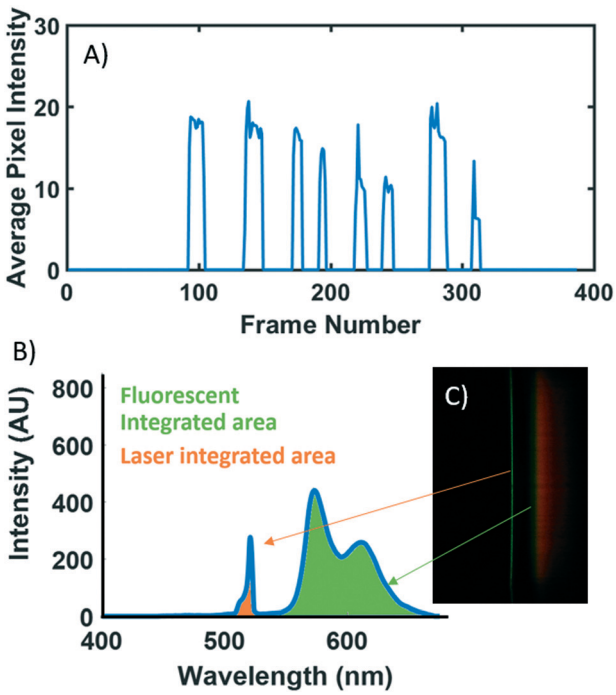

Fig. 7 Video processing and normalization. A) Average pixel intensity of a data-collection video showing clear demarcation of 8 sample wells. B and C) Example fluorescent spectrum showing regions used to normalize the data.

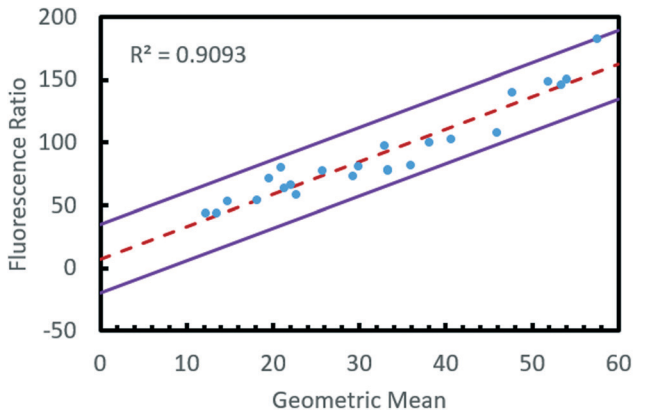

Fig. 8 Bland–Altman analysis of spectral TRI-analyzer compared with standard microplate reader for readout of phenylalanine assay. A variation on the standard Bland–Altman method using the geometric mean and log difference was applied to all non-zero values for each assay (Bland). The log differences showed a dependence on the magnitude of the measurement, so a regressive approach was used to model the relation, as described by Bland (mean of regression shown with dashed line). One point was found to be outside the ±1.96 S.D. limits of agreement (solid lines).

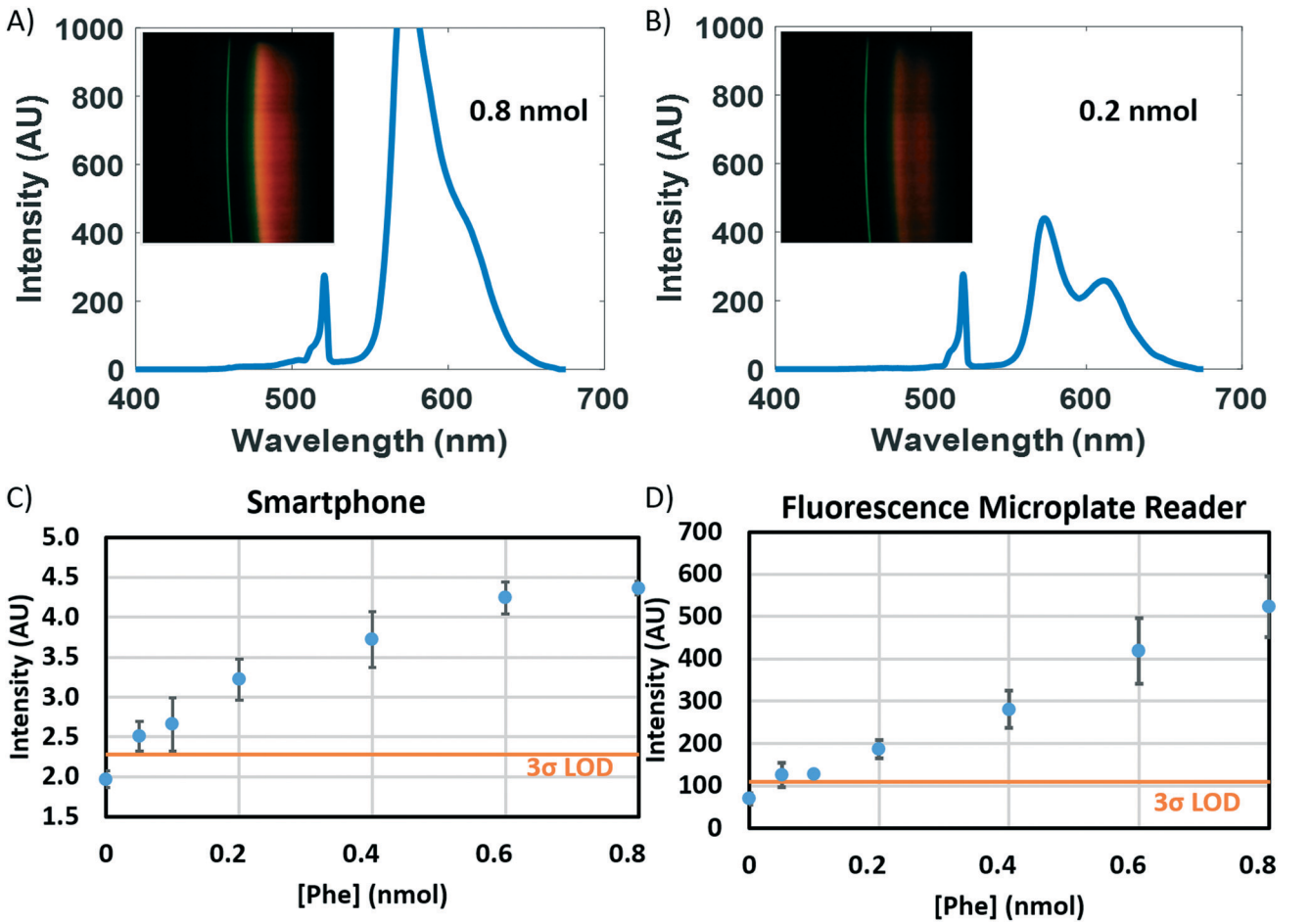

Fig. 9 Results of phenylketonuria assay. A) and B) Sample transmission spectra, absorption spectra, and raw RGB image data (insets) for 0.8 and 0.2 nmol samples of phenylalanine, respectively. C) and D) Comparative dose–response curves for spectral TRI-analyzer and 96-well microplate reader. Standard concentrations from 0 to 8 nmol were assayed. Limit of detection was determined as 3 standard deviations over the mean of zero concentration standard (n = 3).

spectral dimension (Fig. 4C). The result is a spectrum where pixel distance corresponds directly to wavelength, a relationship that can be interpolated from measuring two known lasers with the smartphone system and interpolating the wavelengths in between (Fig. 4C). Finally, to adjust for overall intensity variation resulting from imperfect cartridge alignment with the optical path, a linear scaling least-squares fit was performed on the spectrum above 500 nm (outside the region of interest of our chromogen absorbance) when compared to a broadband spectrum (measured with ultrapure water). Resultant normalized transmission spectra were subtracted from the same broadband spectrum, resulting in absorption spectra (Fig. 5). Similar limits of detection were observed between the 96-well microplate reader and spectral TRI-analyzer, both well under the minimum assay detection range (25 ng mL^{-1}), with the lowest discernable assayed concentration being 37.0 and 12.3 ng mL^{-1}, respectively. Bland–Altman analysis was performed on the measurements from the 96-well plate reader and the spectral TRI-analyzer, and all data were shown to be well within the 95% confidence intervals (Fig. 6).

Intensity light path: phenylalanine fluorescent assay

The prevention of phenylketonuria-associated mental deficits been recognized at one of the largest public health successes of the past 50 years with over 4000 lives saved since screening methods began in the US 50 years ago.[35] Global prevalence is regionally varied, ranging from 1/200 000 in Finland to 1/2600 in Turkey.[36] Traditional newborn screening techniques are based on a heel prick, originally used for bacterial metabolic assay, but now often run *via* mass spectroscopy.[37–39] Benefits of translating newborn birth screening tests to a smartphone-based point-of-care device including cloud-integration and data storage, familiarity of user-interface, cost-effectiveness and portability, directly map to challenges identified by the US Department of Health and Human Services, including the feasibility of statewide surveillance, tracking, and reporting, the roles and responsibilities of a broad and varied user base, and the cost and number of tests needed.[40]

A commercially available assay kit was purchased (Sigma Aldrich) for the quantification of human phenylalanine. The phenylalanine standard was reconstituted in water, and

serially diluted to concentrations of 0.8, 0.6, 0.4, 0.2, 0.1, 0.05, and 0 nmol per well. Human serum samples were deproteinized using a 10 kDa MWCO spin filter before being diluted with assay buffer and added to wells in triplicate (n = 3). The samples were pre-treated for 10 minutes at room temperature with tyrosinase to control for background interference. A sample/standard reaction mixture of developer, enzyme mix, and buffer was added to each of the wells per manufacturer directions. The solutions were allowed to incubate, covered and protected from light, for 20 minutes at 37 C. Using a commercially available 96-well microplate reader (BioTek, Synergy HT), the completed assay was measured for fluorescence, exciting at λ = 535 nm and measuring at λ = 587 nm. Samples were then transferred to cartridges, as described previously, and measured for fluorescence using the spectral TRI-analyzer.

For data acquisition of the fluorescence data, an improved data collection procedure was developed. For absorption-based measurements, the stability of light output is time insensitive; however, with fluorescent dyes, both excitation intensity variation resulting from commercial laser diodes (even after circuit-based feedback control) and fluorophore photobleaching result in a time-dependence of our measurements. To mitigate these variances, we developed a post-processing method that allows us to capture data as a video as the user slides the cartridge through the cradle, thereby reconstituting the spatial dimension in which the multiple sample chambers are introduced into the light path. By analyzing mean pixel value across each frame of the video, contiguous framesets of signal corresponding to each of the sample chambers in the cartridge could be identified (Fig. 7). The center 80% of these frames were averaged, and used as an image to generate a spectrum, as done with the ELISA data. These spectra were then normalized using the measured integrated area of the excitation laser of the sample chambers before assay completion. This normalization method was validated using Bland–Altman analysis (Fig. 8). The resultant fluorescence spectra resulted in a clear dose–response curve with a comparable limit of detection to that of the commercially available plate reader (Fig. 9). The limit of detection for the spectral TRI-analyzer was less than the lowest assayed concentration (0.5 nmol), while the limit of detection for the 96-well plate reader was between 0.5 nmol and 1.0 nmol. We observe saturation of our signal at higher analyte concentrations, suggesting our system may have a lower dynamic range than the microplate reader.

Conclusion

Our unique spectral TRI-analyzer system demonstrates both the breadth of IVD assay possibilities and applications that can be achieved within a single instrument. Each of the three optical biosensing modalities offers up a wide array of existing assays that have been developed for the laboratory setting that can be rapidly translated to be used with such a POCT device.

The development of this device takes advantage of both the rapid improvements to smartphone hardware and software as well as the significant improvements in resolution and affordability of SLA-based 3D printing. This demonstration paves the way for a variety of prototyping applications in optical system design where 3D-printed optical mounts could augment or even replace conventional benchtop optical assembly and alignment. In particular, within the realm of optical biosensors designed for the point-of-care, this presents significant potential to create new optical systems that can proceed from computer simulation directly to handheld prototype.

Similarly, we have demonstrated a rapid-prototype-friendly method for micro- and milli-fluidic cartridges for use with mobile biosensing devices. By linearizing fluid chambers into multi-sample cartridges, we can provide simple multiplexing which is useful both for assays requiring multiple standards or controls, or situations where many samples might be run at once. The simplicity of our laser-cut acrylic sheet and DSA assembly opens the door for a myriad of other possible cartridge configurations, including increasing the number of sample chambers per cartridge for further multiplexing, or incorporating other microfluidic assay steps such as sample lysis, mixing, or other mainstays of microfluidic-chip based technology. For example, the specific dimensions and layout of our cartridges was designed to maximize convenience for interfacing between the assay solutions run on our benchtop comparison instruments that used a 96-well plate format by having sample ports spaced and sized to match the end of an 8-well multichannel pipette.

In the demonstration of our system with existing commercial assays we sought to exemplify the sorts of laboratory-grade tests that could be directly transferred to the point-of-care. Thousands of these kits exist that rely on optical readout of sandwich immunoassays with either absorbance or fluorescence-based reporting molecules (ELISA, FIA, CLIA), and many new assays are being developed based upon other novel techniques, including those using bioluminescence, SPR, PCs or other selective-resonance phenomena.

Video-based capture of sample signals is a natural complement to our developed linear cartridge, further simplifying multi-analyte multiplexing into a more user-friendly interface. This represents a novel data collection method that represents yet another natural benefit of harnessing extant smartphone imaging technology for spectral analysis and biosensing applications. To our knowledge, no such video-based multiplexing of spectral data has been described. The developed image processing holds potential for further expansion into future devices that can take advantage of such a 'swipe' based interface. The swiping of a credit card is a ubiquitous motion that readily simplifies multiplexed sample measurements compared to those in a typical cuvette-based measurement system.

The presented results of both proof-of-concept assays demonstrate that the spectral TRI-analyzer can replicate the sensitivity of conventional benchtop laboratory instruments. In both assays, our smartphone-based system could detect

concentrations of assayed analyte less than those detected on a conventional laboratory instrument. The single largest compromise observed with our system was a decrease in dynamic range for the assays. In the fFN experiment, near-complete absorption of light at 450 nm at high concentrations resulted in signal saturation. For this particular assay, this would likely be acceptable as threshold ranges from literature range from 10–200 ng mL^{-1}.[41–43] Similarly, in the phenylalanine assay, our instrument did not produce a linear dose–response curve, instead demonstrating a saturation–curve relationship at higher concentrations. Likely using a 4-parameter logistic growth curve instead of a linear fit would allow for appropriate unknown concentrations to be determined using our system, but as shown by our Bland–Altman analysis for this data, even the unknown concentration in our serum sample was shown to be measured with agreement between it and our benchtop analyzer. This level of agreement was demonstrated for both assays at all concentrations, suggesting that our device can successfully reproduce the expected assay measurements from identical samples.

A key challenge in developing any successful IVD for use at the point-of-care is achieving a device that is financially feasible. To construct a single system, the cost of components of our system was approximately $550. Many previous proof-of-concept demonstrations have focused on a single usage case, which significantly decreases the cost effectiveness of any diagnostic device. The broad applicability of our device provides a necessary linkage between this previous work and the future possibility of truly portable IVD devices. Demonstrated here is just one example set of related tests that individually might not result in a commercially viable IVD device, but together, provide a powerful opportunity to distribute maternal and child health monitoring from central laboratories to clinics and health outposts worldwide. The potential for this device to function as the backbone of a portable laboratory promises to revolutionize the future of mobile health diagnostics.

Acknowledgements

We would like to acknowledge the National Science Foundation for their support of this work *via* Grant no. CBET 12-64377 and the National Institutes of Health Grant F30AI122925. Additionally, we would like to express our gratitude for the assistance of P. T. Clark for his assistance with the initial optical layout.

Notes and references

1 Frost & Sullivan, *Global Battery Market for Wearables*, 2016.
2 S. A. Soper, K. Brown, A. Ellington, B. Frazier, G. Garcia-Manero, V. Gau, S. I. Gutman, D. F. Hayes, B. Korte, J. L. Landers, D. Larson, F. Ligler, A. Majumdar, M. Mascini, D. Nolte, Z. Rosenzweig, J. Wang and D. Wilson, *Biosens. Bioelectron.*, 2006, **21**, 1932–1942.
3 J. Kirkwood, *The Next Step for Molecular Point-of-Care Testing*, 2016.
4 L. Bissonnette and M. G. Bergeron, *Clin. Microbiol. Infect.*, 2016, **16**, 1044–1053.
5 C. D. Chin, V. Linder and S. K. Sia, *Lab Chip*, 2012, **12**(12), 2118–2134.
6 E. McLeod and A. Ozcan, *Rep. Prog. Phys.*, 2016, **79**, 076001.
7 S. A. Lee and C. Yang, *Lab Chip*, 2014, **14**(16), 3056–3063.
8 H. Yu, Y. Tan and B. T. Cunningham, *Anal. Chem.*, 2014, **86**(17), 8805–8813.
9 M. A. Hossain, J. Canning, S. Ast, K. Cook, P. J. Rutledge and A. Jamalipour, *Opt. Lett.*, 2015, **40**(8), 1737–1740.
10 K. D. Long, H. Yu and B. T. Cunningham, *Biomed. Opt. Express*, 2014, **5**(11), 3792–3806.
11 L. Jiang, M. Mancuso, Z. Lu, G. Akar, E. Cesarman and D. Erickson, *Sci. Rep.*, 2014, **4**, 4137.
12 O. Mudanyali, S. Dimitrov, U. Sikora, S. Padmanabhan, I. Navruz and A. Ozcan, *Lab Chip*, 2012, **12**(15), 2678–2686.
13 A. St John and C. P. Price, *Clin. Biochem. Rev.*, 2014, **35**, 155–167.
14 L. Kwon, K. D. Long, Y. Wan, H. Yu and B. T. Cunningham, *Biotechnol. Adv.*, 2016, **34**, 291–304.
15 D. Zhang and Q. Liu, *Biosens. Bioelectron.*, 2016, **75**, 273–284.
16 H. Zhu, I. Sencan, J. Wong, S. Dimitrov, D. Tseng, K. Nagashima and A. Ozcan, *Lab Chip*, 2013, **13**, 1282–1288.
17 D. Ji, H. Song, N. Zhang, Q. Gan, S. Pi, S. Jiang and X. Zeng, *Front. Opt.*, 2016, DOI: 10.1364/FIO.2016.JW4A.30.
18 M. Seydack, *Biosens. Bioelectron.*, 2005, **20**, 2454–2469.
19 K. A. Willets and R. P. Van Duyne, *Annu. Rev. Phys. Chem.*, 2007, **58**, 267–297.
20 J.-Y. Yoon, *Biol. Eng.*, 2008, **1**, 79–94.
21 M. F. Pineda, L. L.-Y. Chan, T. Kuhlenschmidt, C. J. Choi, M. Kuhlenschmidt and B. T. Cunningham, *IEEE Sens. J.*, 2009, **9**, 470–477.
22 D. Gallegos, K. D. Long, H. Yu, P. P. Clark, Y. Lin, S. George, P. Nath and B. T. Cunningham, *Lab Chip*, 2013, **13**(11), 2124–2132.
23 Frost & Sullivan, *Advances in Label-Free Detection*, Report D12D, 2008.
24 R. Tiwari, *Immunoassay Market Growth Driven by ELISA to Hit 8.2% CAGR to 2021*, 2016.
25 Frost & Sullivan, *Overview of the In-vitro Diagnostics Market in India*, 2013.
26 Frost & Sullivan, *Analysis of the US Immunochemistry Market*, Report NE6F, 2014.
27 WHO, *Health in 2015: from MDGs to SDGs*, World Health Organization, 2015.
28 WHO, *From MDGs to SDGs, WHO launches new report*, World Health Organization, 2016.
29 WHO, *Preterm birth*, World Health Organization, 2016.
30 WHO, *WHO recommendations on interventions to improve preterm birth outcomes*, World Health Organization, 2015.
31 D. G. Kiefer and A. M. Vintzileos, *Rev. Obstet. Gynecol.*, 2008, **1**, 106–112.
32 F. Audibert, S. Fortin, E. Delvin, A. Djemli, S. Brunet, J. Dube and W. D. Fraser, *J. Obstet. Gynaecol. Can.*, 2010, 307–312.
33 D. S. Abbott, S. K. Radford, P. T. Seed, R. M. Tribe and A. H. Shennan, *Am. J. Obstet. Gynecol.*, 2013, **208**, 122.

34 S. Deshpande, A. V. Asselt, F. Tomini, N. Armstrong, A. Allen, C. Noake, K. Khan, J. Severens, J. Kleijnen and M. Westwood, *Health Technol. Assess.*, 2013, **17**(40), 1–138.
35 CDC, *Second National Report on Biochemical Indicators of Diet and Nutrition in the US Population*, Centers for Disease Control, 2012.
36 R. A. Williams, C. D. Mamotte and J. R. Burnett, in *Clin Biochem Rev*, 2008, vol. 29, pp. 31–41.
37 Medical Research Council Working Group, *Br. Med. J.*, 1968, **4**, 7–13.
38 K. Bhattacharya, T. Wotton and V. Wiley, *Transl. Pediatr.*, 2014, **3**, 63–70.
39 E. J. Schoen, J. C. Baker, C. J. Colby and T. T. To, *Pediatrics*, 2002, **110**, 781–786.
40 A. R. Kemper, C. A. Kus, R. J. Ostrander, A. M. Comeau, C. A. Boyle, D. Dougherty, M. Y. Mann, J. R. Botkin and N. S. Green, *Implementing Point-of-Care Newborn Screening*, US Department of Health and Human Services, 2012.
41 H. Leitich and A. Kaider, *BJOG*, 2003, **110**(Suppl 20), 66–70.
42 D. S. Abbott, N. L. Hezelgrave, P. T. Seed, J. E. Norman, A. L. David, P. R. Bennett, J. C. Girling, M. Chandirimani, S. J. Stock, J. Carter, R. Cate, J. Kurtzman, R. M. Tribe and A. H. Shennan, *Obstet. Gynecol.*, 2015, **125**, 1168–1176.
43 G. C. Lu, R. L. Goldenberg, S. P. Cliver, U. S. Kreaden and W. W. Andrews, *Obstet. Gynecol.*, 2001, **97**, 225–228.

